Article

Cell Stem Cell

Runx1 Deficiency Decreases Ribosome Biogenesis and Confers Stress Resistance to Hematopoietic Stem and Progenitor Cells

Graphical Abstract

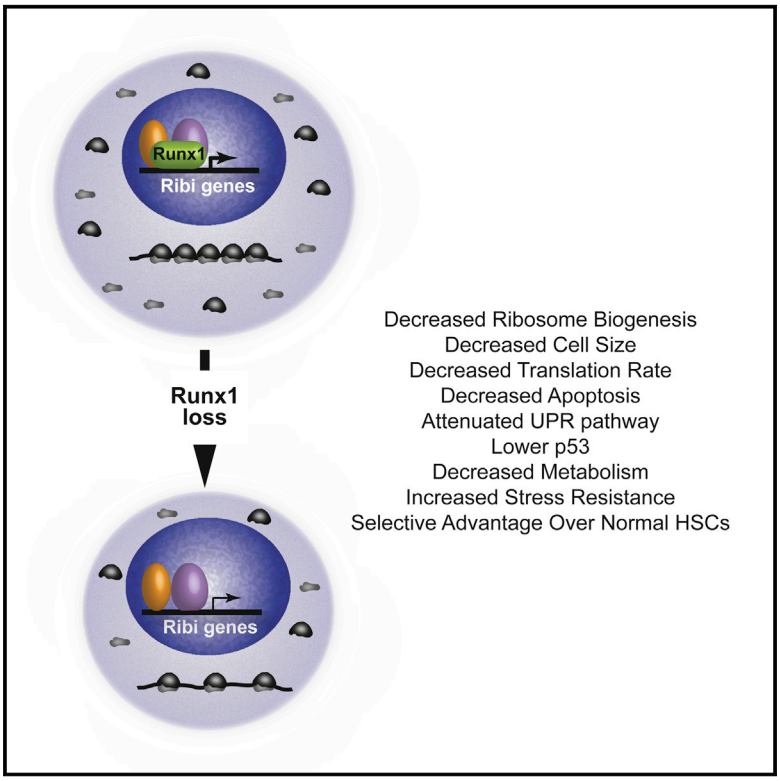

Authors

Xiongwei Cai, Long Gao, Li Teng, ..., Philip J. Mason, Kai Tan, Nancy A. Speck

Correspondence

nancyas@exchange.upenn.edu

In Brief

Loss-of-function *RUNX1* mutations are common in myelodysplastic syndrome and leukemia and can be early events. Cai et al. demonstrate that Runx1 loss decreases ribosome biogenesis and translation in hematopoietic stem and progenitor cells and confers resistance to endogenous and genotoxic stress.

Highlights

- Runx1-deficient HSCs are resistant to endogenous and genotoxic stress
- Runx1-deficient HSCs have decreased ribosome biogenesis
- Runx1 directly regulates ribosome biogenesis

Accession Numbers

GSE67609

Cai et al., 2015, Cell Stem Cell *17*, 165–177
August 6, 2015
http://dx.doi.org/10.1016/j.stem.2015.06.002

Cell Stem Cell
Article

Runx1 Deficiency Decreases Ribosome Biogenesis and Confers Stress Resistance to Hematopoietic Stem and Progenitor Cells

Xiongwei Cai,[1] Long Gao,[2] Li Teng,[3] Jingping Ge,[4] Zaw Min Oo,[1] Ashish R. Kumar,[5] D. Gary Gilliland,[1,6] Philip J. Mason,[4] Kai Tan,[3] and Nancy A. Speck[1,*]
[1]Abramson Family Cancer Research Institute, Institute for Regenerative Medicine and Department of Cell and Developmental Biology, University of Pennsylvania, Philadelphia, PA 19104, USA
[2]Department of Biomedical Engineering, University of Iowa, Iowa City, IA 52242, USA
[3]Department of Internal Medicine, University of Iowa, Iowa City, IA 52242, USA
[4]Department of Pediatrics, The Children's Hospital of Philadelphia, Philadelphia, PA 19104, USA
[5]Division of Bone Marrow Transplantation and Immune Deficiency, Cincinnati Children's Hospital Medical Center, Cincinnati, OH 45229, USA
[6]Abramson Family Cancer Research Institute and Department of Medicine, University of Pennsylvania, Philadelphia, PA 19104, USA
*Correspondence: nancyas@exchange.upenn.edu
http://dx.doi.org/10.1016/j.stem.2015.06.002

SUMMARY

The transcription factor *RUNX1* is frequently mutated in myelodysplastic syndrome and leukemia. *RUNX1* mutations can be early events, creating preleukemic stem cells that expand in the bone marrow. Here we show, counterintuitively, that Runx1-deficient hematopoietic stem and progenitor cells (HSPCs) have a slow growth, low biosynthetic, small cell phenotype and markedly reduced ribosome biogenesis (Ribi). The reduced Ribi involved decreased levels of rRNA and many mRNAs encoding ribosome proteins. Runx1 appears to directly regulate Ribi; Runx1 is enriched on the promoters of genes encoding ribosome proteins and binds the rDNA repeats. Runx1-deficient HSPCs have lower p53 levels, reduced apoptosis, an attenuated unfolded protein response, and accordingly are resistant to genotoxic and ER stress. The low biosynthetic activity and corresponding stress resistance provides a selective advantage to Runx1-deficient HSPCs, allowing them to expand in the bone marrow and outcompete normal HSPCs.

INTRODUCTION

Myelodysplastic syndrome (MDS) and acute myelogenous leukemia (AML) begin with the acquisition of a driver mutation that generates a preleukemic stem cell (pre-LSC) (Pandolfi et al., 2013). The pre-LSC is self-renewing and capable of competing with normal hematopoietic stem cells (HSCs) to ensure its survival and expansion in the bone marrow. Additional mutations gradually accumulate in the pre-LSC and its downstream progeny, giving rise to MDS or AML (Welch et al., 2012). Early mutations in the leukemogenic process often occur in genes encoding chromatin regulators such as *TET2*, *DNMT3A*, *IDH2*, and *ASXL1* (Welch et al., 2012; Xie et al., 2014). These genes mediate processes such as DNA methylation, histone modification, or chromatin looping, altering the epigenetic "landscape" of the pre-LSC (Corces-Zimmerman et al., 2014; Jan et al., 2012; Shlush et al., 2014). Mutations that activate signal transduction pathways, such as internal duplication of *FLT3* are also common in AML, but most often occur as later events in downstream progenitor populations (Corces-Zimmerman et al., 2014).

RUNX1 is a DNA binding transcription factor that is mutated in de novo and therapy-related AML, MDS, chronic myelomonocytic leukemia, acute lymphocytic leukemia, and in the autosomal dominant pre-leukemia syndrome familial platelet disorder with predisposition to acute myeloid leukemia (FPD/AML) (Mangan and Speck, 2011). In mice, loss-of-function (LOF) *Runx1* mutations cause defects in lymphocyte and megakaryocytic development, and alterations in hematopoietic stem and progenitor cells (HSPCs) that include an increase in the number of committed erythroid/myeloid progenitors and expansion of the lineage-negative (L) $Sca1^+$ Kit^+ (LSK) population in the bone marrow (Cai et al., 2011; Growney et al., 2005; Ichikawa et al., 2004). Runx1 deficiency has only a modest adverse effect on the number of functional long-term repopulating hematopoietic stem cells (LT-HSCs), reducing their frequency in the bone marrow by 3-fold at most, without affecting their self-renewal properties (Cai et al., 2011; Jacob et al., 2010). LOF *RUNX1* mutations may also confer increased resistance to genotoxic stress, because several small-scale studies of MDS/AML patients who were previously exposed to radiation or treated with alkylating agents revealed a high incidence (~40%) of somatic single nucleotide variants or insertion/deletion mutations in *RUNX1*, as compared to the overall 6%–10% of MDS patients with LOF *RUNX1* mutations (Bejar et al., 2011; Haferlach et al., 2014; Harada et al., 2003; Walter et al., 2013; Zharlyganova et al., 2008). The higher association of *RUNX1* mutations with exposure to genotoxic agents suggests two possibilities: either *RUNX1* mutations are preferentially induced by these agents, or more likely, that pre-existing *RUNX1* mutations conferred a selective advantage to pre-LSCs exposed to these agents. *RUNX1* mutations can be early or later events in the progression of MDS and AML (Jan et al., 2012; Welch et al., 2012). That they can be early events is demonstrated unequivocally by the observation that

FPD/AML patients who harbor germline mutations in *RUNX1* have an ~35% lifetime risk of developing MDS/AML (Ganly et al., 2004; Michaud et al., 2002; Song et al., 1999).

Although it has been demonstrated that mutations that occur in pre-LSCs cause them to selectively expand in the bone marrow (Busque et al., 2012; Xie et al., 2014), the mechanisms underlying this phenomenon are not well understood. Here we aimed to elucidate the molecular mechanisms by which LOF *RUNX1* mutations generate an expanded population of HSPCs. Counterintuitively, we find that Runx1 deficiency in HSPCs results in a slow growth, low biosynthetic, small cell phenotype, accompanied by markedly decreased ribosome biogenesis (Ribi). Furthermore, Runx1-deficient HSPCs have lower levels of p53 and an attenuated unfolded protein response and are less apoptotic following exposure to genotoxic stress. These observations lead to a model whereby LOF *RUNX1* mutations generate stress-resistant HSPCs that are able to perdure and expand by virtue of their slow growth properties and decreased rates of apoptosis as compared to normal HSPCs.

RESULTS

We previously demonstrated that Runx1-deficient murine HSPCs have a decreased percentage of apoptotic cells (Cai et al., 2011). To determine if Runx1 deficiency also protects against radiation-induced apoptosis, we generated hematopoietic-specific LOF *Runx1* alleles with Vav1-Cre (Cai et al., 2011). We irradiated control *Runx1*$^{f/f}$ (*f/f*) and *Runx1*$^{f/f}$*; Vav1-Cre* (Δ/Δ) mice and measured the percentage of apoptotic HSPCs 24 hr later. HSPCs were analyzed using CD34 and Flt3 markers, because we previously showed that CD48 and CD150 are dysregulated on Runx1-deficient HSPCs (Cai et al., 2011). Staining for Kit was not performed as its levels decrease following irradiation (Simonnet et al., 2009). A smaller percentage of irradiated Δ/Δ CD34$^-$ Flt3$^-$ LS (long-term repopulating HSCs) and CD34$^+$ Flt3$^-$ LS cells (short-term HSCs) were Annexin V$^+$ compared to *f/f* HSCs (Figures 1A and 1B). Runx1 deficiency did not, however, reduce the sensitivity of CD34$^+$ Flt3$^+$ LS cells (multipotent progenitors, MPPs) to radiation. Because reduced apoptosis and other properties to be discussed later were common to both CD34$^+$ Flt3$^-$ and CD34$^-$ Flt3$^-$ LSK cells, these two populations were combined (Flt3$^-$ LSK cells or Flt3$^-$ LS cells in experiments involving radiation or ≥24 hr of in vitro culture) in most experiments.

To determine if Runx1 deficiency provides a selective advantage to HSCs following radiation exposure, we mixed bone marrow (BM) cells from *f/f* or Δ/Δ mice with wild-type competitor BM (+/+) at a 3:4 ratio, and either transplanted the cells directly into lethally irradiated (9Gy) recipient mice, or first subjected the cells to a low level of irradiation (2 Gy) prior to transplantation (Figure 1C). If donor HSCs are less sensitive to radiation than +/+ competitor HSCs, the ratio of donor to +/+ competitor cells should increase following irradiation. The ratio of non-irradiated *f/f* donor to +/+ competitor cells in peripheral blood (PB), total BM, Mac1$^+$ BM cells, and LSK BM cells was the same as the input 3:4 ratio, and not altered by radiation (Figure 1D). In contrast, Δ/Δ LSK cells expanded in the BM relative to +/+ competitor cells ($p \leq 0.002$) (Figure 1E), as previously reported (Cai et al., 2011; Chen et al., 2009; Growney et al., 2005; Ichikawa et al., 2004; Jacob et al., 2010; Motoda et al., 2007). Radiation further increased the percentage of Δ/Δ donor-derived total BM and BM LSK cells relative to non-irradiated Δ/Δ cells, and there was a trend toward increased BM Mac1$^+$ cells (Figure 1E). Therefore, Runx1-deficient HSCs have a selective advantage over normal HSCs that is accentuated by irradiation.

LOF *RUNX1* mutations in AML are associated with refractory disease and inferior event-free, relapse-free, and overall survival, presumably due to chemotherapy resistance (Gaidzik et al., 2011; Tang et al., 2009). To determine if Runx1 deficiency protects HSCs from chemotherapeutic agents, mice were treated for 5 days with arabinofuranosyl cytidine (Ara-C) and apoptosis analyzed. Ara-C treatment increased the percentage of apoptotic CD34$^-$ Flt3$^-$ LS cells of both genotypes, but the percentage of Annexin V$^+$ cells was lower in Δ/Δ than in *f/f* HSCs (Figures 1F–1H).

The expansion and decreased apoptosis of Runx1-deficient HSCs in the absence of induced stress suggests that they are also resistant to endogenous stress. Tunicamycin induces ER stress by blocking N-linked glycosylation, which causes misfolded proteins to accumulate in the ER and trigger the unfolded protein response (UPR). Treatment of mice with tunicamycin induced apoptosis of both *f/f* and Δ/Δ Flt3$^-$ LSK cells, but to a much lesser extent in Δ/Δ cells (Figure 1I). The expression of several UPR response genes was induced following irradiation, but activation of *Atf6*, *Ddit3* (CHOP), and *Xbp1* was significantly attenuated in Δ/Δ Flt3$^-$ LS cells (Figure 1J). Because Δ/Δ HSPCs have a slow growth phenotype and do not exhibit increased self-renewal in serial transplant experiments (Cai et al., 2011), we conclude that their expansion in the BM likely results from their increased resistance to endogenous and genotoxic stress.

Runx1-Deficient HSCs Have Decreased Ribosome Content

We noticed during the course of our analyses that Δ/Δ HSPCs produced less forward scatter (FSC) than *f/f* HSCs, indicating they are smaller in size. This was observed for Δ/Δ CD34$^-$ Flt3$^-$ LSK (LT-HSCs), CD34$^+$ Flt3$^-$ LSK (ST-HSCs), and LKS$^-$ (progenitor) cells, although not for CD34$^+$ Flt3$^+$ LSK cells (MPPs) (Figures 2A and 2B), which coincidentally had normal levels of apoptosis (Figures 1A and 1B). Δ/Δ HSCs also had a smaller diameter than *f/f* HSCs (Figure 1C). To determine if this small cell phenotype was also relevant in humans, we analyzed CD117$^+$ CD34$^+$ BM cells from two FPD/AML patients with heterozygous LOF *RUNX1* mutations. CD117$^+$ CD34$^+$ cells from these individuals also produced less FSC as compared to cells from age-matched control patients analyzed in the clinic on the same day, on the same cytometer (Figure 2D). Although the available samples are too few to draw any firm conclusions, the data suggest that human FPD/AML HSPCs are relatively small. Murine HSPCs with a mono-allelic LOF *Runx1* mutation were not, however, smaller than wild-type HSCs (not shown). Cell size is thus one of several aspects of *Runx1* haploinsufficiency in mice that differs from the human FPD/AML phenotype (Sun and Downing, 2004), because mouse and humans appear to have different sensitivities to moderately reduced *Runx1* dosage.

Cell size generally correlates with ribosome biogenesis (Ribi) (Cook and Tyers, 2007); therefore, we measured the amount of

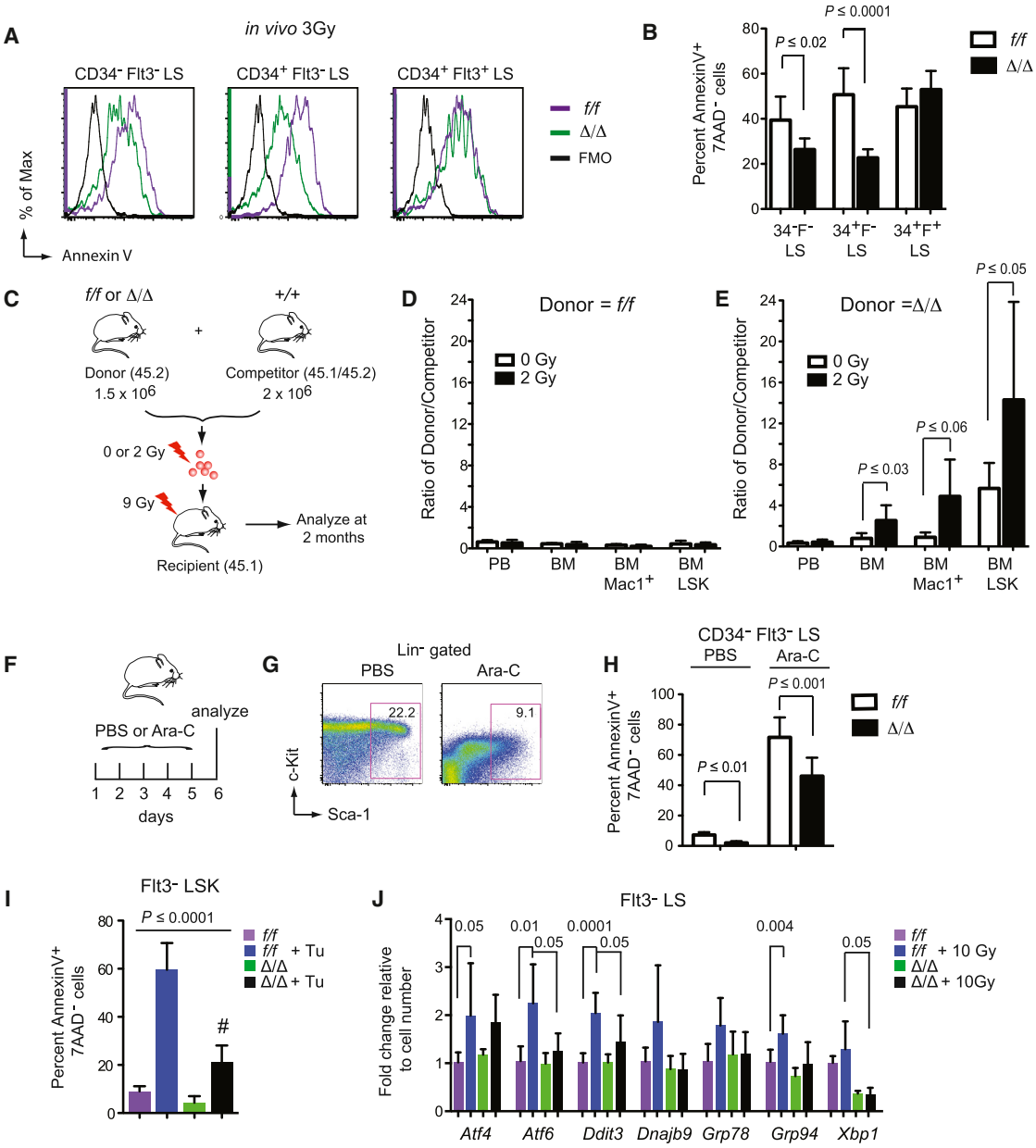

Figure 1. Runx1 Deficiency Protects HSCs from Genotoxic Stress

(A) Apoptosis in phenotypic LT-HSCs (CD34$^-$ Flt3$^-$ LS), ST-HSCs (CD34$^+$ Flt3$^-$ LS), and MPPs (CD34$^+$ Flt3$^+$ LS). Mice were irradiated and 24 hr later 7AAD$^-$ cells analyzed for Annexin V staining. *f/f*, *Runx1*$^{f/f}$; Δ/Δ, *Runx1*$^{f/f}$;*Vav1-Cre*; FMO, fluorescence minus one control.

(B) Summary of data in (A) (mean ± SD, n = 6–7 mice per genotype, unpaired two-tailed Student's t test). 34, CD34; F, Flt3.

(C) In vivo competition experiment. 1.5 × 10^6 *f/f* or Δ/Δ donor BM cells were mixed with 2 × 10^6 wild-type competitor BM cells. The cells were exposed to 0 or 2 Gy radiation then transplanted into recipient mice. Peripheral blood (PB) and BM were analyzed 2 months post-irradiation.

(D) The percentage of *f/f* donor-derived cells [donor/(donor + competitor + residual host)] and +/+ competitor-derived cells [competitor/(donor + competitor + residual host)] is plotted as a ratio of percentage donor/percentage competitor. The experiment was repeated three times, each time using one *f/f* and one Δ/Δ donor. Plotted is a representative experiment (mean ± SD, n = 5–6 recipients, unpaired one-tailed Student's t test).

(E) The percentage of Δ/Δ donor-derived cells divided by the percentage of +/+ competitor cells as in (D). There was a significant expansion in non-irradiated Δ/Δ BM Mac1$^+$ ($p \leq 0.03$) and BM LSK cells ($p \leq 0.03$) compared to their non-irradiated *f/f* counterparts.

(F) Mice were injected for 5 consecutive days with vehicle (PBS) or 10 mg/kg Ara-C, and BM was analyzed on day 6.

(G) Scatter plots show gating for LS cells (Kit was not gated because its levels decreased following Ara-C treatment).

(H) Percentage of apoptotic CD34$^-$ Flt3$^-$ LS cells with or without Ara-C treatment (mean ± SD, n = 7–9 mice, unpaired two-tailed Student's t test).

(I) Percentage of Annexin V$^+$ Flt3$^-$ LSK cells 24 hr post intraperitoneal (i.p.) injection of 1 mg/kg tunicamycin (Tu) or vehicle into mice (mean ± SD, n = 4–7 mice, p value determined by ANOVA; all values are significantly different from the comparator [#] by Dunnett's multiple comparison test).

(J) Expression of UPR transcripts (qPCR) in Flt3$^-$ LS cells with and without 10 Gy irradiation (mean ± SD, n = 3–8 mice, unpaired two-tailed Student's t test).

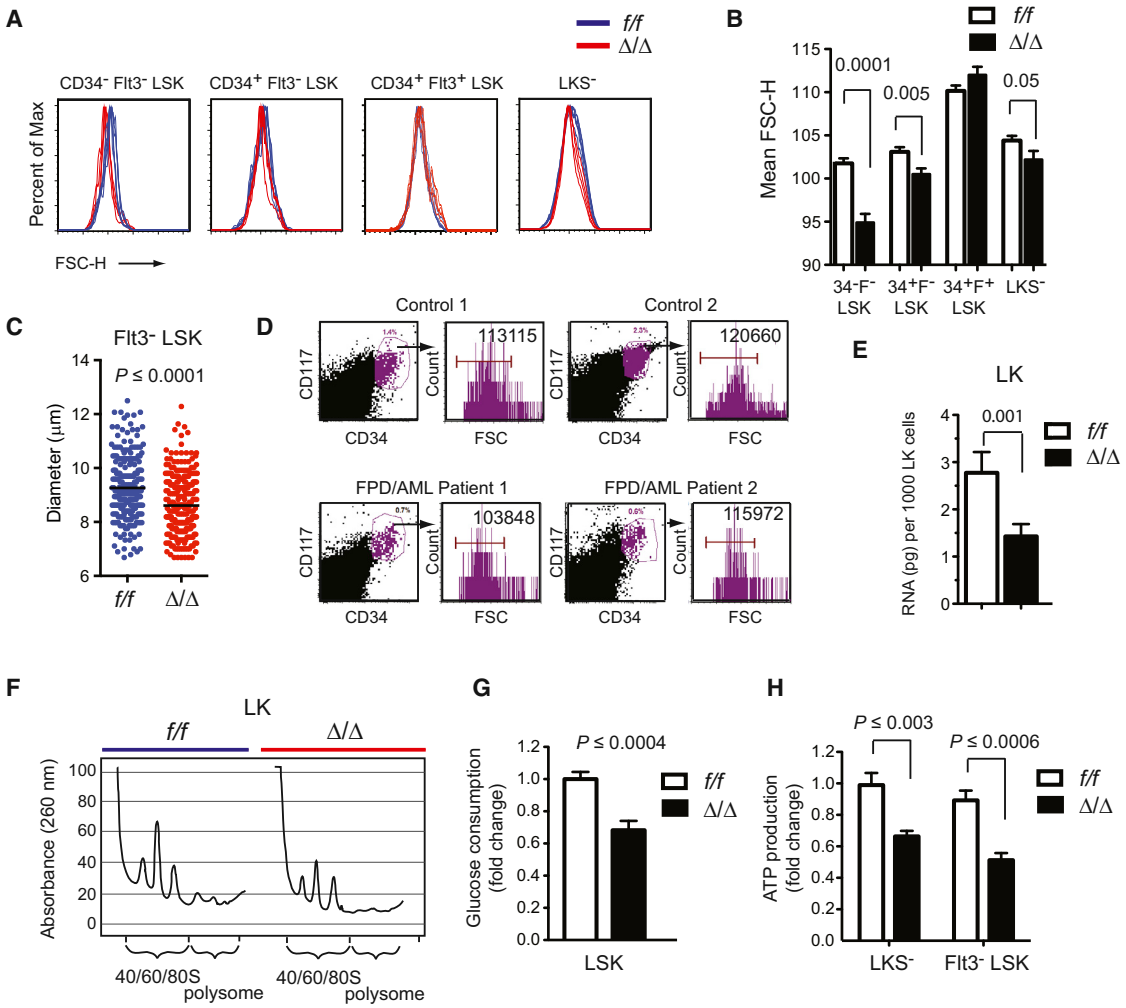

Figure 2. Runx1-Deficient Pre-LSCs Have Decreased Ribosome Biogenesis

(A) Forward scatter analysis of progenitor and HSPC populations.

(B) Summary of data in (A) (mean ± SD, n = 10–12, unpaired two-tailed Student's t test).

(C) Mean diameters of Flt3$^-$ LSK cells, indicated by black lines, p value was determined by unpaired two-tailed Student's t test.

(D) Forward scatter analysis of CD117$^+$ CD34$^+$ BM cells from two FPD/AML patients and two unaffected controls. FPD/AML patient 1 and control 1 were age-matched adults whose BM was analyzed on the same day on the same cytometer in the clinic. FPD/AML patient 2 and control 2 were age-matched children analyzed together on a different day. Mean FSC values are indicated. The FPD/AML patients are heterozygous for a non-functional *RUNX1* allele in which exons 2–6 are duplicated.

(E) Total RNA amount in 1,000 *f/f* and Δ/Δ LK cells (mean ± SD, n = 3–4, unpaired two-tailed Student's t test).

(F) Ribosome profiling. Lysates from 4.5 × 10^6 *f/f* or Δ/Δ cells were lysed and centrifuged through a sucrose gradient.

(G) Glucose consumption of LSK cells. Cells were cultured in 25 mM glucose for 24 hr and the change in glucose concentration in the culture medium measured (mean ± SD, n = 8, unpaired two-tailed Student's t test).

(H) ATP levels in sorted cells (mean ± SD, n = 6, unpaired two-tailed Student's t test).

total RNA in Runx1-deficient cells, as the vast majority (>85%) of cellular RNA comprises or encodes components of the ribosome. Indeed, Runx1-deficient HSPCs (LKS$^{+/-}$, heretofore designated LK) contained 50% less total RNA than *f/f* cells on a per-cell basis (Figure 2E). We also examined ribosome composition by preparing lysates from equal numbers of *f/f* and Δ/Δ LK cells, centrifuging the lysates through a sucrose gradient, and recording the UV absorbance of individual fractions. Δ/Δ LK cells had fewer ribosomes in all fractions, including polysomes, 80S assembled ribosomes, and large and small ribosomal subunits (Figure 2F). Analysis of three separate sucrose gradient experiments showed no perturbation of the 60S/40S subunit ratio, and therefore Ribi was decreased in a balanced manner. Consistent with the decreased Ribi, Runx1-deficient cells had a low metabolic profile; Δ/Δ LSK cells consumed less glucose when cultured in vitro (Figure 2G), and both LKS$^-$ and Flt3$^-$ LSK cells produced less ATP than their *f/f* counterparts (Figure 2H). Runx1 promotes G_1 to S phase cell-cycle progression (Friedman, 2009), and correspondingly Runx1-deficient HSPCs contain a higher percentage of cells in G_1 (Cai et al., 2011). Because decreased

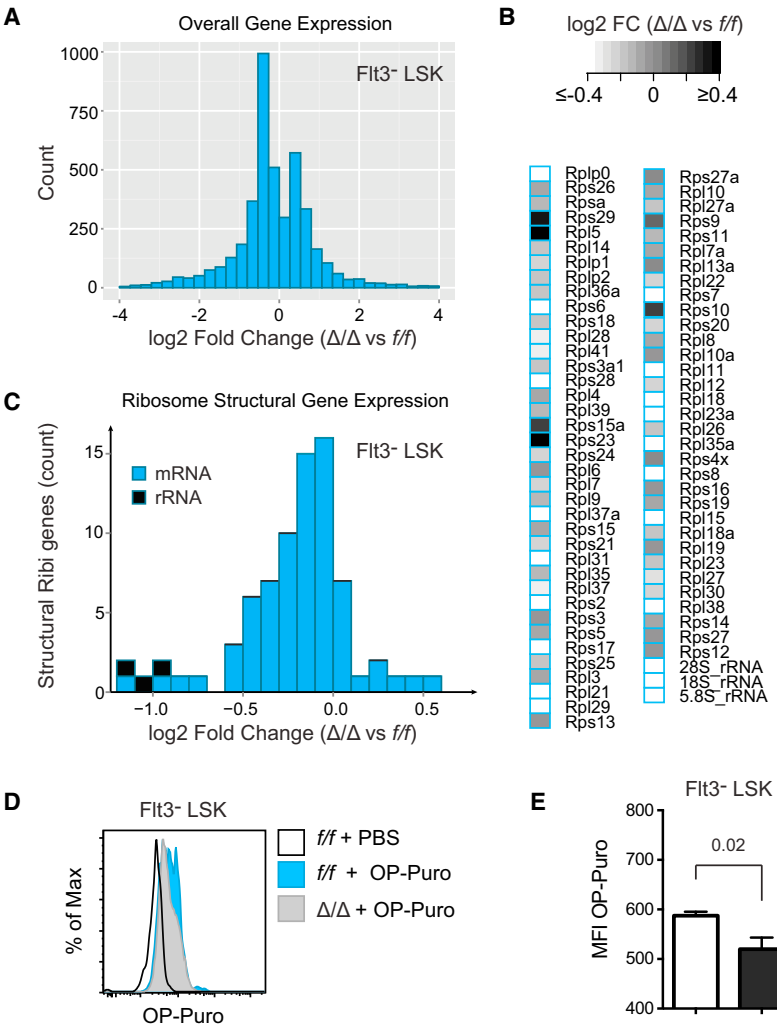

Figure 3. Ribosome Protein and rRNA Transcripts Are Decreased in Δ/Δ HSCs

(A) Histogram of overall gene expression changes in Δ/Δ versus *f/f* Flt3$^-$ LSK cells. Sequencing libraries were prepared from Poly(A) selected RNA from duplicate samples of 2 × 10^4 cells sorted directly into Trizol, with added spike-in controls.

(B) Heatmap of changes in ribosome protein mRNAs and rRNAs. Libraries for rRNA analysis were prepared from total RNA.

(C) Relative expression of genes encoding structural components of ribosomes.

(D) Histogram of OP-Puro incorporation following 1 hour of in vivo labeling.

(E) Summary of OP-Puro incorporation (mean ± SD, n = 7–8, unpaired two-tailed Student's t test). See also Table S1.

Ribi also delays G_1 to S phase progression (Donati et al., 2012), decreased Ribi may underlie the effect of Runx1 deficiency on the cell cycle.

We performed RNA-seq to measure the relative levels of RNAs encoding or comprising structural components of the ribosome, using spike-in controls to normalize the data according to cell number. We made two separate sequencing libraries: one from polyA-selected RNA to analyze mRNAs encoding ribosome proteins, and one from total RNA to compare rRNA levels. In total, 4,248 genes were differentially expressed (FDR < 0.05). There was an average 11% decrease in overall mRNA levels in Δ/Δ Flt3$^-$ LSK cells (Figure 3A), and a slightly greater 13% decrease in mRNA transcripts for ribosome proteins (Figures 3B and 3C). Although an 11% versus 13% difference is small, it was significant ($p < 0.01$, one-tailed t test), indicating that the expression of ribosome protein genes (as compared to all genes) was preferentially affected by Runx1 loss. The largest reduction was in rRNA, which was lower by 51% in Δ/Δ HSCs (Figure 3C), similar to the reduction in total RNA levels in LK cells (Figure 2E).

Decreased biosynthetic capacity should negatively affect the rate of translation. We examined translation by measuring the incorporation of the alkyne puromycin analog O-propargyl-puromycin (OP-Puro) into nascent peptides following injection into mice, as described by Signer et al. (Signer et al., 2014). Δ/Δ Flt3$^-$ LSK cells incorporated significantly less OP-Puro than *f/f* cells, indicating that the overall rate of translation was decreased in Δ/Δ HSCs (Figures 3D and 3E).

Decreased Ribi Can Be Partially Reversed by Activating mTOR Signaling

The mTOR pathway is an important regulator of cell growth, Ribi, and overall translation. Activated mTOR phosphorylates 4EBP1, relieving its repression of eIF4E, allowing Cap-dependent translation initiation (Figure 4A). mTOR also phosphorylates ribosomal protein S6 kinase (S6K), which directly regulates Ribi by phosphorylating the small ribosomal protein S6, and by inactivating several repressors of rRNA and ribosome protein transcription (Huber et al., 2011). The overall levels of S6, 4EBP1, tuberous sclerosis complex 2 (TSC2), and actin were slightly decreased in Δ/Δ LK and Flt3$^-$ LSK cells freshly isolated from the BM (Figure 4B). Phosphorylated 4EBP1 (p-4EBP1) was lower relative to total 4EBP1 raising the possibility that tonic mTOR signaling was slightly dampened. The p-S6 level varied in different experiments; in some experiments it was elevated in Δ/Δ CD34$^{+/-}$ Flt3$^-$ LSK cells (Figure S1), and in other experiments p-S6 was lower (Figure 4B). Although the activation status of tonic mTOR signaling was somewhat equivocal, our interpretation is that it is not greatly decreased and unlikely to account for the ~50% decrease in Ribi.

We examined mTOR signaling further by analyzing mTOR pathway activation in response to hematopoietic cytokines. Runx1 directly regulates several cytokine receptors including MPL, the receptor for thrombopoietin (TPO), an important regulator of HSC function (Cai et al., 2011; Heller et al., 2005; Kimura et al., 1998; Solar et al., 1998). Therefore, we predicted that Runx1-deficient HSPCs might be less responsive to mTOR

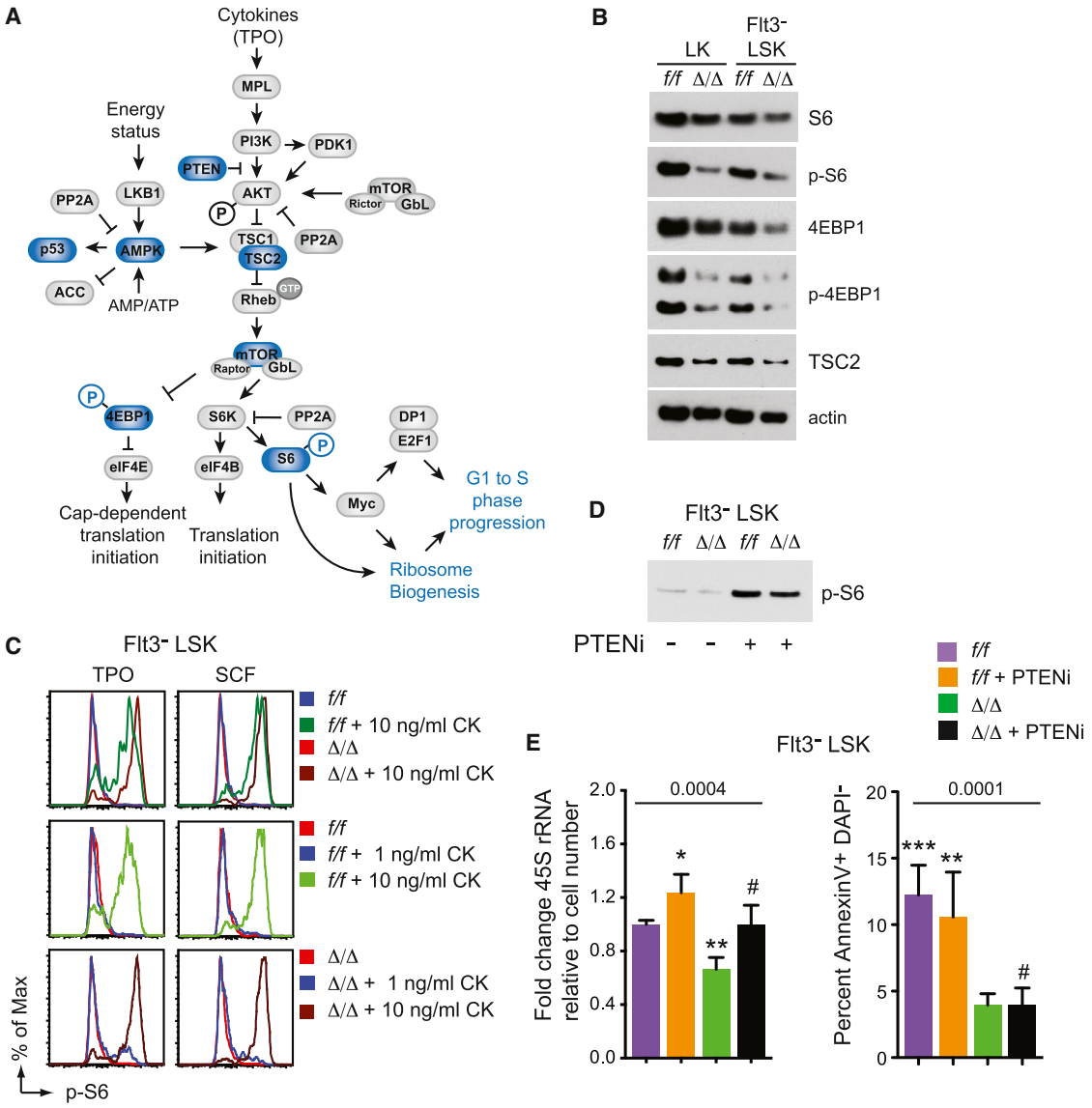

Figure 4. mTOR Signaling in Runx1-Deficient HSPCs

(A) Summary of mTOR pathway. Blue indicates proteins or phosphorylation events that were examined by western blot.

(B) Western blot of mTOR pathway proteins in freshly isolated HSPCs (lysates from 20,000 cells/lane).

(C) Activation of the mTOR pathway as measured by phosphorylation of S6 in serum-starved cells stimulated with SCF or TPO at the indicated concentrations. CK, cytokine.

(D) Western blot for p-S6 in lysates prepared from 20,000 Flt3$^-$ LSK cells 24 hr following i.p. injection of the PTEN inhibitor VO-OHpic trihydrate (PTENi).

(E) Left: qPCR for 45S rRNA in Flt3$^-$ LSK cells 24 hr following i.p. injection of vehicle or PTENi (mean ± SD, n = 3–5 mice). Right: apoptosis in Flt3$^-$ LSK cells following injection of PTENi (mean ± SD, n = 3–6 mice). The p values determined by one-way ANOVA; values significantly different from the comparators (#) by Dunnett's multiple comparison test are indicated with asterisks.

See also Figure S1.

activation by cytokines. We tested the response of Δ/Δ Flt3$^-$ LSK cells to TPO, and also to stem cell factor (SCF) to determine if this was the case. The addition of 10 ng/ml TPO or SCF to serum-starved *f/f* and Δ/Δ Flt3$^-$ LSK cells in vitro resulted in S6 phosphorylation within 10 min (Figure 4C). Contrary to our prediction, the mean fluorescence intensity (MFI) of p-S6 was higher in Δ/Δ Flt3$^-$ LSK cells relative to *f/f* cells following TPO or SCF stimulation. *f/f* and Δ/Δ Flt3$^-$ LSK cells also responded to similar concentrations of TPO and SCF (Figure 4C). We conclude that the mTOR pathway could be robustly activated by TPO and SCF in Δ/Δ Flt3$^-$ LSK cells.

Activation of mTOR signaling can correct some of the proliferation, differentiation, and translation defects associated with mutations in ribosome protein genes (Boultwood et al., 2013; Payne et al., 2012). To determine whether activation of mTOR signaling could reverse the decreased Ribi and apoptosis in

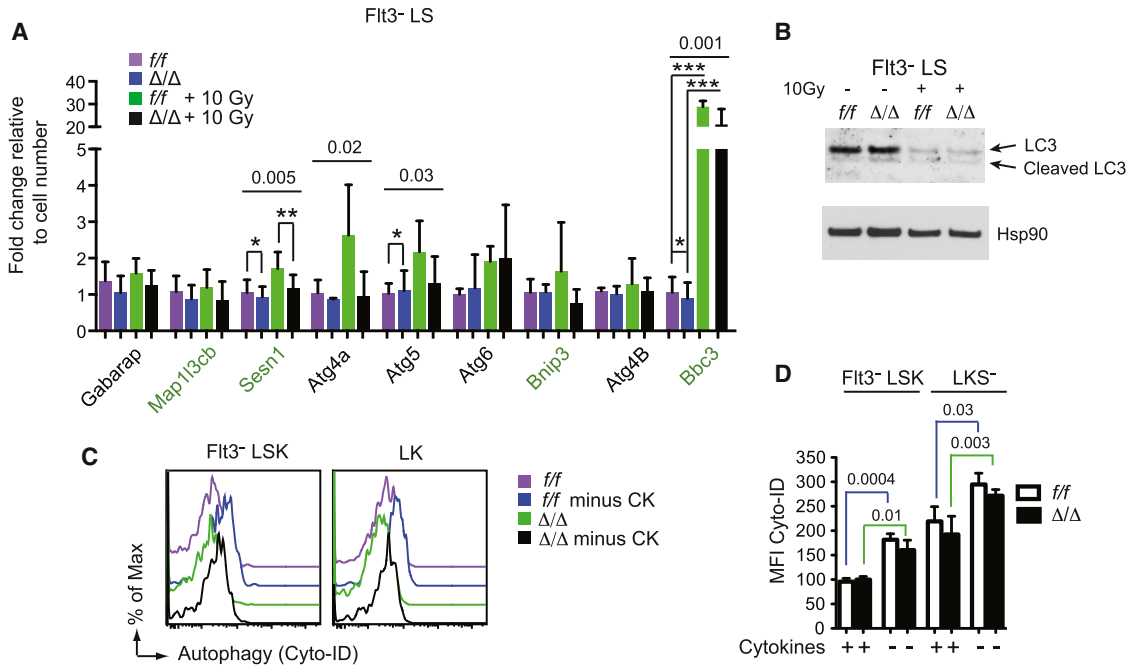

Figure 5. Runx1-Deficient HSPCs Do Not Undergo Increased Autophagy

(A) Relative mRNA levels for core (black labels) and pro-autophagy genes (green labels) in freshly isolated Flt3$^-$ LS cells without or 24 hr post-10-Gy radiation (mean ± SD, n = 3–8, p value determined by one-way ANOVA, significantly different values were determined by Bonferroni's multiple comparison test and indicated with asterisks).

(B) Western blot for LC3 in lysates prepared from 20,000 Flt3$^-$ LS cells without or 6-hr post-10-Gy radiation.

(C) Autophagy in HSPCs measured by Cyto-ID staining of autophagic vacuoles. Cells were cultured for 6 hr in the presence or absence of cytokines (CK represents SCF, Flt3L, IL-11). Fresh cells or starved cells were stained by Cyto-ID.

(D) Quantification of data in (B) (mean ± SD, n = 3 for two experiments; shown is one representative experiment, unpaired two-tailed Student's t test).

Δ/Δ HSCs, we treated mice with an inhibitor of phosphatase and tensin homolog (PTEN), VO-OHpic trihydrate (PTENi). Injection of PTENi increased p-S6 levels in both *f/f* and Δ/Δ Flt3$^-$ LSK cells, demonstrating that mTOR signaling was activated (Figure 4D). Activation of mTOR signaling increased the levels of 45S rRNA in both *f/f* and Δ/Δ Flt3$^-$ LSK cells (Figure 4E), although 45S rRNA levels were still significantly lower in Δ/Δ compared to *f/f* cells. Activation of mTOR had no effect on the percentage of apoptotic *f/f* or Δ/Δ Flt3$^-$ LSK cells (Figure 4E), thus increased mTOR signaling could partially normalize Ribi, but it failed to alter the low apoptotic phenotype of Δ/Δ HSCs.

Increased Autophagy Does Not Contribute to Decreased Ribi

Autophagy is a process by which cellular contents, including ribosomes, are degraded and recycled for use under starvation conditions. Lower mTOR signaling can induce autophagy, which in turn could contribute to the decreased ribosome content of Δ/Δ cells. We analyzed the expression of genes encoding the core autophagy machinery and several genes whose expression defines a pro-autophagic signature (Warr et al., 2013) by qPCR. Expression of the pro-autophagy signature genes was either unaltered (*Bnip3*) or slightly lower (*Sesn1*, *Bbc3*) in Δ/Δ Flt3$^-$ LS cells (Figure 5A). Radiation increased *Bbc3* (Puma) mRNA in both *f/f* and Δ/Δ Flt3$^-$ LS cells, but significantly less so in Δ/Δ cells (Figure 5A). The proportion of cleaved versus uncleaved LC3 protein, which is required for the formation of autophagosomal membranes, increased to a similar extent in irradiated *f/f* and Δ/Δ Flt3$^-$ LS cells (Figure 5B). We measured autophagy in Flt3$^-$ LSK cells and LKS$^-$ progenitors that were provided or starved for cytokines by labeling autophagic vacuoles (pre-autophagosomes, autophagosomes, and autolysosomes) with a cationic amphiphilic tracer dye, Cyto-ID. Cytokine starvation increased the staining of autophagic vacuoles in both *f/f* and Δ/Δ Flt3$^-$ LSK and LK cells, indicative of increased autophagy (Figures 5C and 5D). However, the autophagic vacuolar staining was equivalent in Δ/Δ and *f/f* cells in the presence or absence of cytokines. We conclude that increased autophagy is not the primary cause of the decreased ribosome content in Δ/Δ HSCs and progenitors. Because mTOR signaling represses autophagy, and autophagy is not higher in Δ/Δ HSCs, this supports our conclusion that tonic mTOR signaling is not significantly decreased in Δ/Δ HSCs.

Runx1 Directly Regulates Ribi

Because alterations in mTOR signaling and autophagy did not explain the decreased Ribi, we concluded there was another explanation, and we examined whether Runx1 directly regulates Ribi. We analyzed the genome-wide occupancy of RUNX1 using previously published chromatin immunoprecipitation sequencing (ChIP-seq) data generated in human CD34$^+$ HSPCs (Beck et al., 2013). We identified 20,552 RUNX1 peaks (q value < 0.01) and examined peaks located within 5 kb of the transcriptional start sites (TSS) of their closest genes (32.37% of all

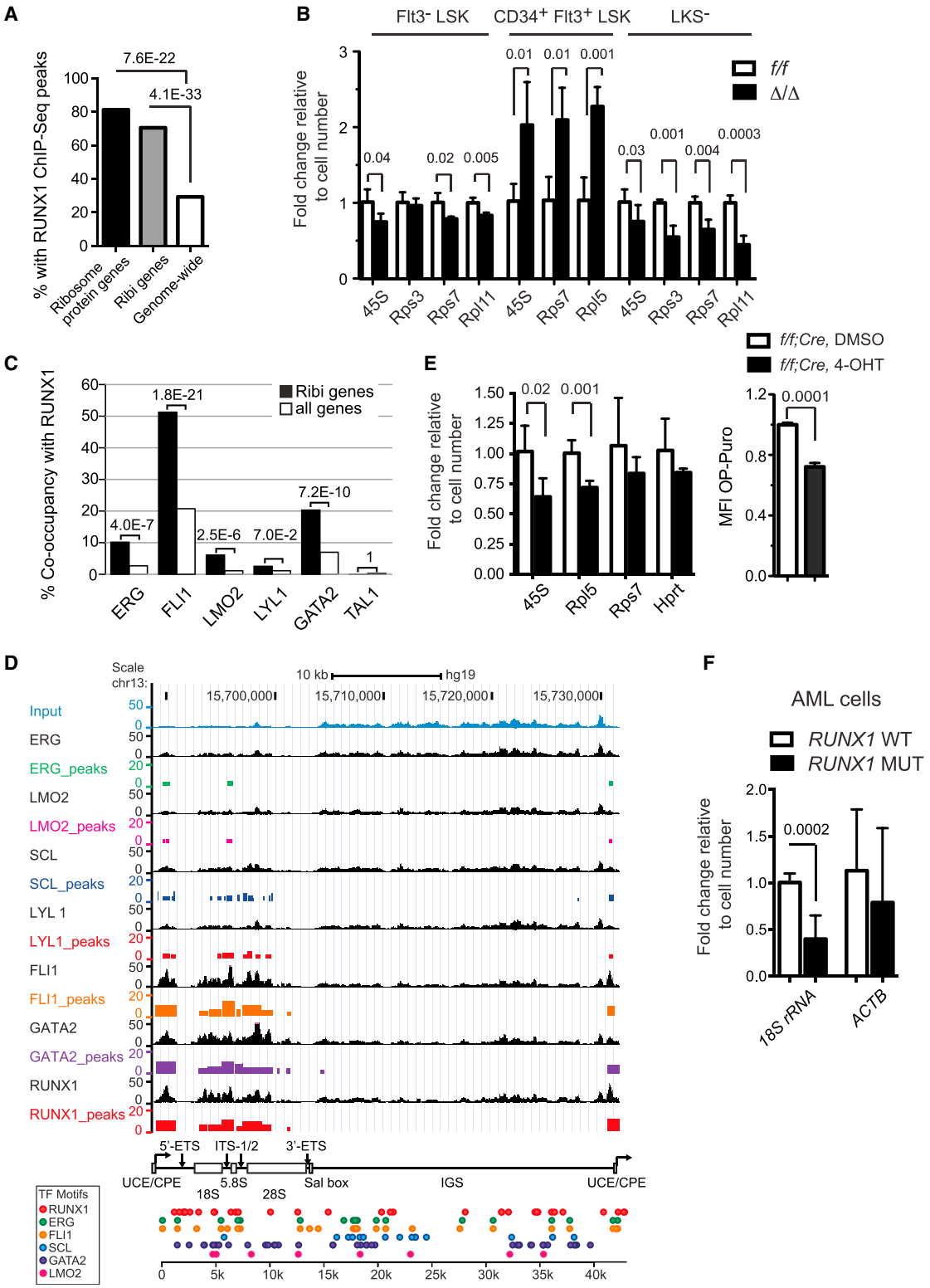

Figure 6. Runx1 Is Enriched at the Promoters of Ribosome Protein Genes and Occupies rDNA Repeats

(A) Enrichment of Runx1 binding peaks at the promoters of ribosome protein genes and genes involved in Ribi. Enrichment p value is shown over the bars and was computed using hypergeometric distribution. Genes annotated with biological process gene ontology terms related to Ribi plus 80 ribosome protein genes were analyzed.

(B) qPCR for rRNA and ribosome protein mRNAs in HSPCs (mean ± SD n = 3–5, unpaired two-tailed Student's t test).

(legend continued on next page)

RUNX1 peaks); we found that 70.56% of the promoter proximal regions of 197 genes involved in Ribi, which included 80 genes encoding large or small ribosome subunit proteins, were occupied by RUNX1 in human CD34$^+$ HSPCs (Figure 6A). Of the 80 genes encoding structural proteins of the ribosome, 65 (80.25%) had a RUNX1 peak within 5 kb of their promoter (Figure 6A). An additional 45 Ribi genes, including ten ribosome protein genes, had at least one RUNX1 peak with an enrichment of $\geq$2-fold over input (Table S1). In comparison, only 29.3% of all promoters genome-wide were occupied by RUNX1 (Figure 6A). Therefore RUNX1 binding in human CD34$^+$ HSPCs is highly enriched at the promoters of Ribi genes ($p \leq 4.1 \times 10^{-33}$), including the subset of Ribi genes encoding structural components of the ribosome ($p \leq 7.6 \times 10^{-22}$). We performed a similar analysis of Runx1 occupancy using other published ChIP-seq datasets, and although the fraction of Ribi genes occupied by Runx1 was lower in these other cell types and studies, in all cases occupancy was enriched on Ribi genes (Table S2). We examined the expression of several ribosome genes occupied by RUNX1 in more purified populations of mouse HSPCs, and found significant differences in the levels of *Rps3*, *Rps7*, *Rpl11*, and rRNA transcripts in both Δ/Δ Flt3$^-$ LSK and LK(S$^-$) cells when measured on a per-cell basis (Figure 6B). Interestingly, the expression of *Rps7* and 45S rRNA was elevated in Δ/Δ Flt3$^+$ LSK cells (MPPs), and thus the effect of Runx1 loss on Ribi is context dependent. In conclusion, many genes involved in Ribi are direct Runx1 targets, and their expression is affected by an LOF Runx1 mutation.

We next determined whether other hematopoietic transcription factors (TFs), including GATA2, FLI1, LYL1, TAL1, LMO2, and ERG, were enriched on RUNX1-bound promoters in human CD34$^+$ HSPCs (Beck et al., 2013). We found that FLI1 was highly enriched on RUNX1-occupied Ribi gene promoters; approximately 50% of the Ribi gene promoters bound by RUNX1 were also occupied by FLI1, as compared to 20% of the RUNX1-bound promoters genome-wide (Figure 6C). GATA2 was also highly enriched on Ribi gene promoters bound by RUNX1, although to a lesser extent than FLI1 (Figure 6C). Enrichment of ERG and LMO2 co-occupancy was significant, whereas co-occupancy by LYL1 and TAL1 was not enriched.

In addition to occupying the promoters of ribosome protein genes, all three Runx proteins (Runx1, Runx2, and Runx3) were previously shown to associate with nucleolar organizing regions, to bind RUNX consensus sites in the genes encoding rRNA (rDNA), and to regulate rRNA transcription (Ali et al., 2008; Young et al., 2007). We analyzed the binding of RUNX1 and the other hematopoietic TFs to the rDNA repeats using the same ChIP-seq data generated in hCD34$^+$ HSPCs (Beck et al., 2013). Current genome assemblies do not contain rDNA repeats, so in order to map ChIP-seq reads to the rDNA sequence we computationally appended the sequence of a single rDNA repeat to the proximal tip of chromosome 13 in the human genome assembly. Because only one rDNA repeat sequence is included in the assembly, the data obtained represent an aggregate of signals on all ~400 rDNA repeats (Zentner et al., 2011). All seven TFs occupied the upstream control element/core promoter element (UCE/CPE), and most of the rDNA repeat coding region, with RUNX1, GATA2, and FLI1 generating the most highly enriched peaks (Figure 6D). The occupied regions were similar to those bound by the second largest subunit of DNA polymerase I (RPA116) and the upstream binding protein (UBF) in K562 cells (Zentner et al., 2011). Analysis of the rDNA repeat sequence identified motifs for the five sequence-specific TFs (RUNX1, GATA2, FLI1, TAL1, and ERG) throughout the rDNA repeat, including in the intergenic sequence (IGS) not occupied by any of the TFs based on the lack of enrichment relative to input (Figure 6D).

We examined whether acute deletion of Runx1 would affect the levels of 45S rRNA and translational rate in HSPCs. Purified HSCs (Flt3$^-$ LSK) containing two floxed *Runx1* alleles and a tamoxifen-regulated Cre (Hayashi and McMahon, 2002) were cultured ex vivo for 48 hr in the presence or absence of the tamoxifen metabolite 4-hydroxytamoxifen (4-OHT). The level of 45S rRNA and OP-Puro incorporation were significantly reduced 48 hr after deletion of *Runx1* with Cre + 4-OHT (Figure 6E), further supporting the hypothesis that Runx1 directly regulates Ribi in HSPCs. We also analyzed the level of rRNA in primary human AML cells containing LOF *RUNX1* mutations. 18S rRNA was significantly lower in AML cells containing LOF *RUNX1* mutations, suggesting that the relatively low Ribi phenotype is also a feature of AML blasts (Figure 6F).

In summary, the Ribi gene promoter and rDNA occupancy data derived in human CD34$^+$ cells, in addition to the effects of acute deletion of Runx1 on 45S rRNA levels and translation in HSPCs, support a direct role for Runx1 in regulating Ribi.

Runx1-Deficient HSPCs Do Not Activate p53

Ribi is the most energy-consuming cellular process, and its integrity is carefully monitored by a p53 checkpoint. Defects associated with the ribosomopathies Diamond-Blackfan anemia (DBA), Schwachman-Diamond syndrome, and in the somatically acquired 5q− syndrome in MDS caused by mutations in Ribi genes result in activation of p53, G_1 growth arrest, and cellular

(C) Enrichment of co-occurrence of RUNX1 and other hematopoietic TFs at the promoters of Ribi genes. The p values were computed using hypergeometric distribution.

(D) TF ChIP-seq peaks across the rDNA sequence. For each TF, the top track shows the normalized ChIP-seq signal and the bottom track shows binding peaks called by MACS2. The height of a peak is proportional to the fold enrichment of the ChIP-seq signal compared to input control. On the bottom are TF binding sites across the rDNA sequence. Binding sites were detected using FIMO at $p < 0.005$. IGS, intergenic spacer; UCE/CPE, upstream control element/core promoter element; 5′-ETS, 5′ external spacer; ITS-I/2, internal transcribed spacer regions 1 and 2; Sal box; 3′-ETS, 3′ external spacer.

(E) Acute deletion of Runx1 in vitro decreases 45S rRNA and translation. Runx1 was deleted in *Runx1$^{f/f}$* cells that were transgenic for a ubiquitously expressed, tamoxifen regulated Cre, by addition of 4-OHT to the culture medium. Left: RNA levels were measured by qPCR 48 hr after 4-OHT addition (mean ± SD, n = 5). Right: OP-Puro incorporation (mean ± SD, n = 3; p values determined by unpaired two-tailed Student's t test).

(F) rRNA levels in primary human AML cells with (MUT) or without (WT) LOF *RUNX1* mutations (mean ± SD, n = 5–7, unpaired two-tailed Student's t test).

See also Tables S1 and S2.

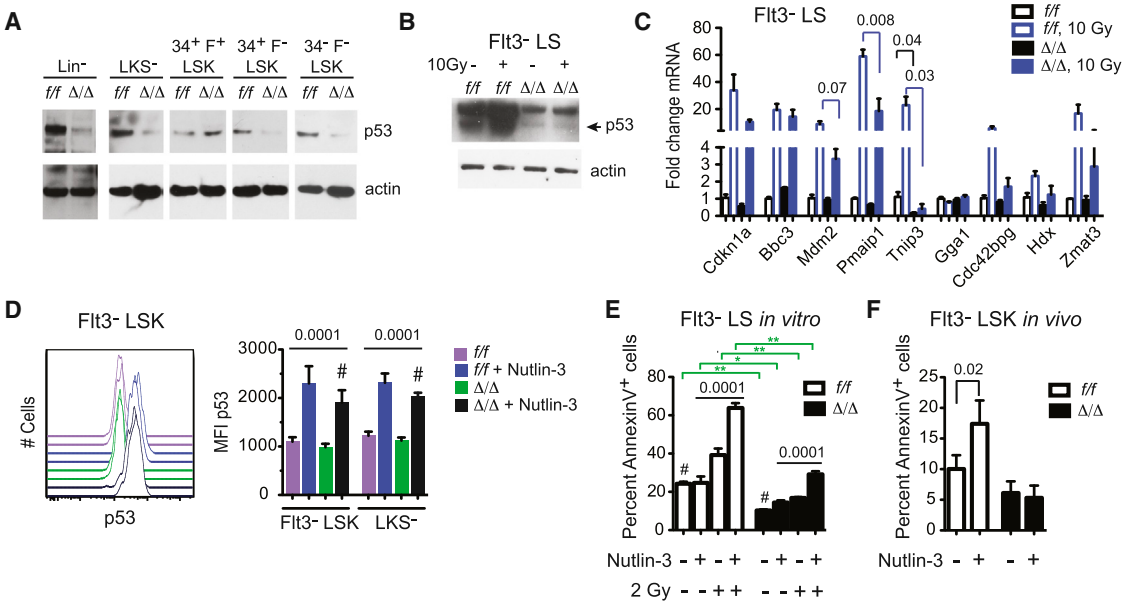

Figure 7. p53 Protein Levels Are Lower in Runx1-Deficient HSPCs

(A) Western blots for p53 in purified HSC and progenitor populations. Lysates from 20,000 cells were loaded in each lane. The p53 and actin blots are different exposures from the same gel.

(B) p53 in Flt3$^-$ LS cells, pre- and 6 hr post-radiation of mice.

(C) qRT-PCR for p53 target genes in Flt3$^-$ LS cells, pre- and 6 hr post-radiation or mice (mean ± SEM, n = 3, unpaired two-tailed Student's t test).

(D) Intracellular p53 staining in HSPCs in the absence or presence of Nutlin-3 treatment in vitro (3 hr at 10 μM). On left are representative histograms for Flt3$^-$ LSK cells. Data for Flt3$^-$ LSK and LKS$^-$ cells are summarized in the bar graph on the right (mean ± SD, n = 5, one-way ANOVA, all values were significantly different from the comparators [#] by Dunnett's multiple comparison test).

(E) Annexin V$^+$ Flt3$^-$ LS cells in the absence and presence of Nutlin-3 and irradiation in vitro (mean ± SD, n = 5, ANOVA and Dunnett's multiple comparison tests, comparator [#]). Significant differences between pairs of samples are indicated by green brackets and determined by unpaired two-tailed Student's t test.

(F) Annexin V$^+$ Flt3$^-$ LSK cells in mice 24 hr post-i.p. injection of Nutlin-3 (20 mg/kg) (mean ± SD, n = 4, unpaired two-tailed Student's t test).

senescence or apoptosis (Golomb et al., 2014). However, we observed lower p53 protein levels in Δ/Δ versus the corresponding *f/f* populations in western blots of lysates prepared from equal numbers of HSPCs, including Lineage minus (Lin$^-$) and LKS$^-$ progenitors, LT-HSCs, and ST- HSCs (Figure 7A). *Tp53* mRNA levels were not altered, however, in Δ/Δ Flt3$^-$ LSK cells by RNA-seq; therefore, the reduction in p53 protein levels in LT-HSCs and ST-HSCs occurs post-transcriptionally. The only population in which p53 was not reduced was CD34$^+$ Flt3$^+$ LSK cells (MPPs) (Figure 7A), which correlated with their normal size (Figures 2A and 2B), higher levels of 45S rRNA (Figure 6B), and lack of radiation resistance (Figures 1A and 1B). Radiation increased p53 levels in *f/f* Flt3$^-$ LS cells, but very little increase was observed in the equivalent Δ/Δ population (Figure 7B). The activation of several p53 target genes by radiation (*Mdm2*, *Pmaip1*, and *Tnip3*) was attenuated in Δ/Δ Flt3$^-$ LS cells (Figure 7C).

We determined the extent to which activation of p53 could correct the low apoptotic phenotype of Δ/Δ HSCs by treating cells with the Mdm2-p53 inhibitor Nutlin-3. Treatment with Nutlin-3 increased the levels of p53 in Flt3$^-$ LSK and LKS$^-$ cells, although the p53 MFI was lower in Δ/Δ cells than in equivalently treated *f/f* cells (Figure 7D). Apoptosis was not elevated to the same extent in Δ/Δ Flt3$^-$ LS cells as compared to *f/f* cells in response to Nutlin 3 treatment in vitro, either in the absence or presence or radiation (Figure 7E), and Nutlin 3 failed to increase the percentage of apoptotic Δ/Δ Flt3$^-$ LSK cells in vivo when injected into mice (Figure 7F). In summary, we conclude that the p53 pathway is attenuated in Δ/Δ HSPCs, but that activation of p53 alone cannot reverse the low apoptotic phenotype.

DISCUSSION

LOF *RUNX1* mutations can be early or later events in the progression of MDS or AML. Here we show that early LOF Runx1 mutations reduce Ribi in HSPCs. The reduction in Ribi correlated with lower rates of translation and a stress-resistant phenotype, with attenuated UPR and p53 pathways. The increased stress resistance resulted in the superior survival of Runx1-deficient HSCs in the face of genotoxic insults, providing them with a selective advantage over normal HSCs in the BM. Thus, Runx1 mutations create a "hibernating" pre-LSC that, due to its stress resistance, can perdure and preferentially accumulate. The negative impact of Runx1 loss on Ribi could be partially reversed by activating mTOR signaling, suggesting that one of the important contributions of cooperating mutations in AML that activate signaling pathways may be to at least partially overcome the decreased Ribi. Importantly, activation of mTOR signaling increased Ribi without increasing apoptosis, thus the stress resistance conferred by Runx1 loss persists in the context of proliferative signals, as shown previously for activated Ras signaling

(Motoda et al., 2007). It will be interesting to see if other initiating mutations in MDS and AML result in dysregulation of Ribi, and whether this is a common mechanism underlying pre-malignancy. Evaluation of Ribi in human MDS and AML samples will require normalizing RNA levels based on cell number with spike-in controls because normalizing by total RNA content will mask alterations in Ribi (Lovén et al., 2012).

Although we cannot rule out the possibility that altered expression of cell surface or signaling molecules is responsible for the decreased Ribi, the ChIP-seq occupancy data suggest that Runx1 loss directly affects Ribi. The regulation of Ribi by Runx1 is consistent with previous studies demonstrating that Runx proteins regulate the transcription of rRNA (Ali et al., 2008; Young et al., 2007). However, the prior studies showed that Runx1 functions as a negative regulator of rRNA transcription; here we show that Runx1 appears to positively regulate rRNA transcription in HSCs and progenitors and negatively regulate it in MPPs. Therefore, the functional outcome of Runx1 loss is context dependent. The activity of Runx1 in different contexts may be influenced by cooperating hematopoietic TFs such as FLI1, which was previously shown to regulate Ribi in Friend erythroleukemic cells (Juban et al., 2009), or by global regulators of Ribi such as Myc (Dang, 2012). The chromatin regulatory complexes that Runx1 recruits could also determine whether the outcome is the activation or repression of Ribi. For example, Runx1 recruits the polycomb repressor complex 1 (PRC1) through a direct interaction with Bmi1 (Yu et al., 2012), and loss of Bmi1 decreased the expression of multiple Ribi genes in erythroid progenitor cells (Gao et al., 2015).

The decrease in p53 levels in Runx1-deficient HSPCs is in direct contrast to the activation of p53 associated with perturbed Ribi in the ribosomopathies. Ribosomopathies are caused by mutations in ribosome proteins or assembly factors and are thought to create imbalances in ribosome components, often apparent as an imbalance in the ratio of small and large ribosome subunits (Teng et al., 2013). This in turn leads to the accumulation of excess ribosome proteins that cannot be incorporated into small or large ribosome subunits. Two ribosome proteins, RPL5 and RPL11, are major mediators of this Ribi checkpoint; excess RPL5 and RPL11 bind Mdm2 and inhibit its interaction with p53, causing p53 to accumulate (Teng et al., 2013). However, in situations where both rRNA and mRNAs for ribosome proteins are decreased, p53 levels tend to be lower rather than higher (Donati et al., 2011). For example, simultaneous inhibition of rRNA and protein synthesis by serum starvation or rapamycin treatment was shown to reduce, rather than increase, p53 levels (Donati et al., 2011). In Runx1-deficient HSPCs, both rRNA and mRNAs encoding ribosome proteins were lower, there was no evidence of either small or large ribosome subunit accumulation, and the p53 checkpoint was not activated.

The demonstration of decreased Ribi and the low metabolic profile of Runx1-deficient HSPCs raises the issue of how residual Runx1-deficient leukemic or preleukemic HSCs can be eradicated in patients during or following chemotherapy to reduce bulk disease. Determining how the survival and stress resistance of these cells is wired may be necessary for devising strategies to ablate them.

EXPERIMENTAL PROCEDURES

Mice

Runx1$^{f/f}$;Vav1-Cre mice (8–12 weeks old) were described previously (Cai et al., 2011). Mice were treated according to the University of Pennsylvania's Animal Resources Center and IACUC protocols.

Human Samples

AML pheresis and BM mononuclear cells were obtained from the University of Pennsylvania Stem Cell and Xenograft Core, under the approval from the University of Pennsylvania Institutional Review Board (IRB). All samples lacked *TP53*, *ATM*, *KIT*, *PTEN*, *JAK2*, and *KRAS* mutations. Frozen human AML samples were recovered in RPMI 1640 with 10% fetal bovine serum, live cells counted, and RNA prepared from equivalent numbers of cells. FPD/AML samples were obtained under the approval from the Cincinnati Children's IRB.

Transplantation

B6.SJL (Ly5.1) mice were purchased from the National Cancer Institute and used as recipients. Whole BM cells from 129S1/SvImJ (Ly5.2) × B6.SJL (Ly5.1) F1 mice (JAX) were used as competitors; 2×10^6 competitor cells mixed with 1.5×10^6 *Runx1$^{f/f}$* or *Runx1$^{f/f}$;Vav1-Cre* BM were either irradiated (2 Gy) or not, and injected into the tail veins of irradiated recipient mice (9 Gy, split dose 3 hr apart). BM contribution was measured 2 months after transplantation.

Cell Purification and Flow Cytometry

Followed lineage depletion (Miltenyi), BM cells were stained with surface markers and analyzed/sorted by LSRII/Aria (BD Bioscience). Antibodies are listed in the Supplemental Experimental Procedures. Dead cells were stained with 7-AAD (eBioscience) or DAPI (Invitrogen). VO-OHpic (Sigma) was injected into mice (20 mg/kg i.p.) on 2 consecutive days.

Cell diameters were measured as described elsewhere (Signer et al., 2014).

Intracellular Staining

Cells were fixed by 2% paraformaldehyde, permeabilized by methanol, then incubated with primary (1:300) and secondary antibody (1:2,000). To measure translation rates in vivo, mice were injected with OP-Puro (Medchem Source, 50 mg/kg, i.p.), BM was collected 1 hour later and stained for surface markers and OP-Puro using the Click-iT Protein Synthesis Assay Kit (Life Technologies) (Signer et al., 2014). To measure translation following *Runx1* deletion in vitro, purified Kit$^+$ cells were cultured with 5 μM 4-OHT for 48 hr, and OP-Puro added 20 min before harvesting and staining the cells.

Apoptosis Assays

Mice were killed 24 hr post-radiation with 3 Gy or following a single i.p. injection with tunicamycin (Sigma, 1 mg/kg) or Nutlin-3 (Sigma, 20 mg/kg), or after the last of five daily injections with AraC (Sigma, 100 mg/kg). BM cells were stained for Annexin V, DAPI, and antibodies against lineage (B220, CD3, Ter119, Mac1, and Gr1), Sca1, Flt3, CD34, and Kit. Lin$^-$ cells were enriched with a lineage depletion kit (Miltenyi), cultured with or without 10 μM Nutlin-3 for 24 hr, and then stained for cell surface markers.

Autophagy Assay

HSPCs were purified and cultured in Stemspan medium with or without SCF (150 ng/ml), Flt3 (1 ng/ml), and IL-11 (20 ng/ml) for 6 hr. Cyto-ID staining was analyzed following the manufacturer's protocol (Enzo Life Sciences).

Western Blots and qPCR

For this procedure, 2×10^4 sorted cells were mixed with loading dye and electrophoresed through 4%–12% SDS-PAGE gels for western blots. Total RNA was extracted with microRNA easy kit (QIAGEN) and digested with DNase (QIAGEN). Concentration was measured by Bio-analyzer (Agilent). Reverse transcription and real-time PCR were performed using standard protocols. Antibodies, qPCR primer sequences, and a more detailed western blot protocol are included in the Supplemental Experimental Procedures.

Polysome Profiling

A total of 4.5×10^6 Lin$^-$ c-Kit$^+$ cells were sorted and polysome profiling performed using standard protocols.

Glucose Consumption and ATP Production

Sorted LSK cells were cultured for 24 hr in Stem Span medium. Glucose concentration in the medium was measured by YSI 7100 Multiparameter Bioanalytical System (YSI Life Sciences), and ATP in cells using an ATP Detection Kit (Life Technologies).

ChIP-Seq and RNA-Seq

Methods for ChIP-seq and RNA-seq analysis are described in the Supplemental Experimental Procedures.

ACCESSION NUMBERS

The accession number for the RNA-seq data reported in this paper is GEO: GSE67609.

SUPPLEMENTAL INFORMATION

Supplemental Information includes Supplemental Experimental Procedures, one figure, and two tables and can be found with this article online at http://dx.doi.org/10.1016/j.stem.2015.06.002.

ACKNOWLEDGMENTS

NIH R01 CA149976 and the Abramson Family Cancer Research Institute (to N.A.S.), NIH R01 CA106995 (to P.M.), NIH R01 HL111192 (to A.R.K.), and NIH R01 HG006130 (to K.T.) supported this work. Core facilities at the University of Pennsylvania are supported by a Cancer Center Support Grant to the Abramson Cancer Center (P30 CA016520). Technical support was provided by Daniel Marmer of the Diagnostic Immunology Laboratory, Cincinnati Children's Hospital Medical Center.

Received: November 21, 2014
Revised: April 5, 2015
Accepted: June 5, 2015
Published: July 9, 2015

REFERENCES

Ali, S.A., Zaidi, S.K., Dacwag, C.S., Salma, N., Young, D.W., Shakoori, A.R., Montecino, M.A., Lian, J.B., van Wijnen, A.J., Imbalzano, A.N., et al. (2008). Phenotypic transcription factors epigenetically mediate cell growth control. Proc. Natl. Acad. Sci. USA *105*, 6632–6637.

Beck, D., Thoms, J.A., Perera, D., Schütte, J., Unnikrishnan, A., Knezevic, K., Kinston, S.J., Wilson, N.K., O'Brien, T.A., Göttgens, B., et al. (2013). Genome-wide analysis of transcriptional regulators in human HSPCs reveals a densely interconnected network of coding and noncoding genes. Blood *122*, e12–e22.

Bejar, R., Stevenson, K., Abdel-Wahab, O., Galili, N., Nilsson, B., Garcia-Manero, G., Kantarjian, H., Raza, A., Levine, R.L., Neuberg, D., and Ebert, B.L. (2011). Clinical effect of point mutations in myelodysplastic syndromes. N. Engl. J. Med. *364*, 2496–2506.

Boultwood, J., Yip, B.H., Vuppusetty, C., Pellagatti, A., and Wainscoat, J.S. (2013). Activation of the mTOR pathway by the amino acid (L)-leucine in the 5q- syndrome and other ribosomopathies. Adv. Biol. Reg. *53*, 8–17.

Busque, L., Patel, J.P., Figueroa, M.E., Vasanthakumar, A., Provost, S., Hamilou, Z., Mollica, L., Li, J., Viale, A., Heguy, A., et al. (2012). Recurrent somatic TET2 mutations in normal elderly individuals with clonal hematopoiesis. Nat. Genet. *44*, 1179–1181.

Cai, X., Gaudet, J.J., Mangan, J.K., Chen, M.J., De Obaldia, M.E., Oo, Z., Ernst, P., and Speck, N.A. (2011). Runx1 loss minimally impacts long-term hematopoietic stem cells. PLoS ONE *6*, e28430.

Chen, M.J., Yokomizo, T., Zeigler, B.M., Dzierzak, E., and Speck, N.A. (2009). Runx1 is required for the endothelial to haematopoietic cell transition but not thereafter. Nature *457*, 887–891.

Cook, M., and Tyers, M. (2007). Size control goes global. Curr. Opin. Biotechnol. *18*, 341–350.

Corces-Zimmerman, M.R., Hong, W.J., Weissman, I.L., Medeiros, B.C., and Majeti, R. (2014). Preleukemic mutations in human acute myeloid leukemia affect epigenetic regulators and persist in remission. Proc. Natl. Acad. Sci. USA *111*, 2548–2553.

Dang, C.V. (2012). MYC on the path to cancer. Cell *149*, 22–35.

Donati, G., Bertoni, S., Brighenti, E., Vici, M., Treré, D., Volarevic, S., Montanaro, L., and Derenzini, M. (2011). The balance between rRNA and ribosomal protein synthesis up- and downregulates the tumour suppressor p53 in mammalian cells. Oncogene *30*, 3274–3288.

Donati, G., Montanaro, L., and Derenzini, M. (2012). Ribosome biogenesis and control of cell proliferation: p53 is not alone. Cancer Res. *72*, 1602–1607.

Friedman, A.D. (2009). Cell cycle and developmental control of hematopoiesis by Runx1. J. Cell. Physiol. *219*, 520–524.

Gaidzik, V.I., Bullinger, L., Schlenk, R.F., Zimmermann, A.S., Röck, J., Paschka, P., Corbacioglu, A., Krauter, J., Schlegelberger, B., Ganser, A., et al. (2011). RUNX1 mutations in acute myeloid leukemia: results from a comprehensive genetic and clinical analysis from the AML study group. J. Clin. Oncol. *29*, 1364–1372.

Ganly, P., Walker, L.C., and Morris, C.M. (2004). Familial mutations of the transcription factor RUNX1 (AML1, CBFA2) predispose to acute myeloid leukemia. Leuk. Lymphoma *45*, 1–10.

Gao, R., Chen, S., Kobayashi, M., Yu, H., Zhang, Y., Wan, Y., Young, S.K., Soltis, A., Yu, M., Vemula, S., et al. (2015). Bmi1 promotes erythroid development through regulating ribosome biogenesis. Stem Cells *33*, 925–938.

Golomb, L., Volarevic, S., and Oren, M. (2014). p53 and ribosome biogenesis stress: the essentials. FEBS Lett. *588*, 2571–2579.

Growney, J.D., Shigematsu, H., Li, Z., Lee, B.H., Adelsperger, J., Rowan, R., Curley, D.P., Kutok, J.L., Akashi, K., Williams, I.R., et al. (2005). Loss of Runx1 perturbs adult hematopoiesis and is associated with a myeloproliferative phenotype. Blood *106*, 494–504.

Haferlach, T., Nagata, Y., Grossmann, V., Okuno, Y., Bacher, U., Nagae, G., Schnittger, S., Sanada, M., Kon, A., Alpermann, T., et al. (2014). Landscape of genetic lesions in 944 patients with myelodysplastic syndromes. Leukemia *28*, 241–247.

Harada, H., Harada, Y., Tanaka, H., Kimura, A., and Inaba, T. (2003). Implications of somatic mutations in the AML1 gene in radiation-associated and therapy-related myelodysplastic syndrome/acute myeloid leukemia. Blood *101*, 673–680.

Hayashi, S., and McMahon, A.P. (2002). Efficient recombination in diverse tissues by a tamoxifen-inducible form of Cre: a tool for temporally regulated gene activation/inactivation in the mouse. Dev. Biol. *244*, 305–318.

Heller, P.G., Glembotsky, A.C., Gandhi, M.J., Cummings, C.L., Pirola, C.J., Marta, R.F., Kornblihtt, L.I., Drachman, J.G., and Molinas, F.C. (2005). Low Mpl receptor expression in a pedigree with familial platelet disorder with predisposition to acute myelogenous leukemia and a novel AML1 mutation. Blood *105*, 4664–4670.

Huber, A., French, S.L., Tekotte, H., Yerlikaya, S., Stahl, M., Perepelkina, M.P., Tyers, M., Rougemont, J., Beyer, A.L., and Loewith, R. (2011). Sch9 regulates ribosome biogenesis via Stb3, Dot6 and Tod6 and the histone deacetylase complex RPD3L. EMBO J. *30*, 3052–3064.

Ichikawa, M., Asai, T., Saito, T., Seo, S., Yamazaki, I., Yamagata, T., Mitani, K., Chiba, S., Ogawa, S., Kurokawa, M., and Hirai, H. (2004). AML-1 is required for megakaryocytic maturation and lymphocytic differentiation, but not for maintenance of hematopoietic stem cells in adult hematopoiesis. Nat. Med. *10*, 299–304.

Jacob, B., Osato, M., Yamashita, N., Wang, C.Q., Taniuchi, I., Littman, D.R., Asou, N., and Ito, Y. (2010). Stem cell exhaustion due to Runx1 deficiency is prevented by Evi5 activation in leukemogenesis. Blood *115*, 1610–1620.

Jan, M., Snyder, T.M., Corces-Zimmerman, M.R., Vyas, P., Weissman, I.L., Quake, S.R., and Majeti, R. (2012). Clonal evolution of preleukemic hematopoietic stem cells precedes human acute myeloid leukemia. Sci. Transl. Med. *4*, 149ra118.

Juban, G., Giraud, G., Guyot, B., Belin, S., Diaz, J.J., Starck, J., Guillouf, C., Moreau-Gachelin, F., and Morlé, F. (2009). Spi-1 and Fli-1 directly activate

common target genes involved in ribosome biogenesis in Friend erythroleukemic cells. Mol. Cell. Biol. *29*, 2852–2864.

Kimura, S., Roberts, A.W., Metcalf, D., and Alexander, W.S. (1998). Hematopoietic stem cell deficiencies in mice lacking c-Mpl, the receptor for thrombopoietin. Proc. Natl. Acad. Sci. USA *95*, 1195–1200.

Lovén, J., Orlando, D.A., Sigova, A.A., Lin, C.Y., Rahl, P.B., Burge, C.B., Levens, D.L., Lee, T.I., and Young, R.A. (2012). Revisiting global gene expression analysis. Cell *151*, 476–482.

Mangan, J.K., and Speck, N.A. (2011). RUNX1 mutations in clonal myeloid disorders: from conventional cytogenetics to next generation sequencing, a story 40 years in the making. Crit. Rev. Oncog. *16*, 77–91.

Michaud, J., Wu, F., Osato, M., Cottles, G.M., Yanagida, M., Asou, N., Shigesada, K., Ito, Y., Benson, K.F., Raskind, W.H., et al. (2002). In vitro analyses of known and novel RUNX1/AML1 mutations in dominant familial platelet disorder with predisposition to acute myelogenous leukemia: implications for mechanisms of pathogenesis. Blood *99*, 1364–1372.

Motoda, L., Osato, M., Yamashita, N., Jacob, B., Chen, L.Q., Yanagida, M., Ida, H., Wee, H.J., Sun, A.X., Taniuchi, I., et al. (2007). Runx1 protects hematopoietic stem/progenitor cells from oncogenic insult. Stem Cells *25*, 2976–2986.

Pandolfi, A., Barreyro, L., and Steidl, U. (2013). Concise review: preleukemic stem cells: molecular biology and clinical implications of the precursors to leukemia stem cells. Stem Cells Transl. Med. *2*, 143–150.

Payne, E.M., Virgilio, M., Narla, A., Sun, H., Levine, M., Paw, B.H., Berliner, N., Look, A.T., Ebert, B.L., and Khanna-Gupta, A. (2012). L-Leucine improves the anemia and developmental defects associated with Diamond-Blackfan anemia and del(5q) MDS by activating the mTOR pathway. Blood *120*, 2214–2224.

Shlush, L.I., Zandi, S., Mitchell, A., Chen, W.C., Brandwein, J.M., Gupta, V., Kennedy, J.A., Schimmer, A.D., Schuh, A.C., Yee, K.W., et al.; HALT Pan-Leukemia Gene Panel Consortium (2014). Identification of pre-leukaemic haematopoietic stem cells in acute leukaemia. Nature *506*, 328–333.

Signer, R.A., Magee, J.A., Salic, A., and Morrison, S.J. (2014). Haematopoietic stem cells require a highly regulated protein synthesis rate. Nature *509*, 49–54.

Simonnet, A.J., Nehmé, J., Vaigot, P., Barroca, V., Leboulch, P., and Tronik-Le Roux, D. (2009). Phenotypic and functional changes induced in hematopoietic stem/progenitor cells after gamma-ray radiation exposure. Stem Cells *27*, 1400–1409.

Solar, G.P., Kerr, W.G., Zeigler, F.C., Hess, D., Donahue, C., de Sauvage, F.J., and Eaton, D.L. (1998). Role of c-mpl in early hematopoiesis. Blood *92*, 4–10.

Song, W.-J., Sullivan, M.G., Legare, R.D., Hutchings, S., Tan, X., Kufrin, D., Ratajczak, J., Resende, I.C., Haworth, C., Hock, R., et al. (1999). Haploinsufficiency of CBFA2 causes familial thrombocytopenia with propensity to develop acute myelogenous leukaemia. Nat. Genet. *23*, 166–175.

Sun, W., and Downing, J.R. (2004). Haploinsufficiency of AML1 results in a decrease in the number of LTR-HSCs while simultaneously inducing an increase in more mature progenitors. Blood *104*, 3565–3572.

Tang, J.L., Hou, H.A., Chen, C.Y., Liu, C.Y., Chou, W.C., Tseng, M.H., Huang, C.F., Lee, F.Y., Liu, M.C., Yao, M., et al. (2009). AML1/RUNX1 mutations in 470 adult patients with de novo acute myeloid leukemia: prognostic implication and interaction with other gene alterations. Blood *114*, 5352–5361.

Teng, T., Thomas, G., and Mercer, C.A. (2013). Growth control and ribosomopathies. Curr. Opin. Genet. Dev. *23*, 63–71.

Walter, M.J., Shen, D., Shao, J., Ding, L., White, B.S., Kandoth, C., Miller, C.A., Niu, B., McLellan, M.D., Dees, N.D., et al. (2013). Clonal diversity of recurrently mutated genes in myelodysplastic syndromes. Leukemia *27*, 1275–1282.

Warr, M.R., Binnewies, M., Flach, J., Reynaud, D., Garg, T., Malhotra, R., Debnath, J., and Passegué, E. (2013). FOXO3A directs a protective autophagy program in haematopoietic stem cells. Nature *494*, 323–327.

Welch, J.S., Ley, T.J., Link, D.C., Miller, C.A., Larson, D.E., Koboldt, D.C., Wartman, L.D., Lamprecht, T.L., Liu, F., Xia, J., et al. (2012). The origin and evolution of mutations in acute myeloid leukemia. Cell *150*, 264–278.

Xie, M., Lu, C., Wang, J., McLellan, M.D., Johnson, K.J., Wendl, M.C., McMichael, J.F., Schmidt, H.K., Yellapantula, V., Miller, C.A., et al. (2014). Age-related mutations associated with clonal hematopoietic expansion and malignancies. Nat. Med. *20*, 1472–1478.

Young, D.W., Hassan, M.Q., Pratap, J., Galindo, M., Zaidi, S.K., Lee, S.H., Yang, X., Xie, R., Javed, A., Underwood, J.M., et al. (2007). Mitotic occupancy and lineage-specific transcriptional control of rRNA genes by Runx2. Nature *445*, 442–446.

Yu, M., Mazor, T., Huang, H., Huang, H.T., Kathrein, K.L., Woo, A.J., Chouinard, C.R., Labadorf, A., Akie, T.E., Moran, T.B., et al. (2012). Direct recruitment of polycomb repressive complex 1 to chromatin by core binding transcription factors. Mol. Cell *45*, 330–343.

Zentner, G.E., Saiakhova, A., Manaenkov, P., Adams, M.D., and Scacheri, P.C. (2011). Integrative genomic analysis of human ribosomal DNA. Nucleic Acids Res. *39*, 4949–4960.

Zharlyganova, D., Harada, H., Harada, Y., Shinkarev, S., Zhumadilov, Z., Zhunusova, A., Tchaizhunusova, N.J., Apsalikov, K.N., Kemaikin, V., Zhumadilov, K., et al. (2008). High frequency of AML1/RUNX1 point mutations in radiation-associated myelodysplastic syndrome around Semipalatinsk nuclear test site. J. Radiat. Res. (Tokyo) *49*, 549–555.